Article

Biogenic Guanine Crystals Are Solid Solutions of Guanine and Other Purine Metabolites

Noam Pinsk, Avital Wagner, Lilian Cohen, Christopher J. H. Smalley, Colan E. Hughes, Gan Zhang, Mariela J. Pavan, Nicola Casati, Anne Jantschke, Gil Goobes, Kenneth D. M. Harris, and Benjamin A. Palmer*

Read Online

ACCESS | Metrics & More | Article Recommendations | SI Supporting Information

ABSTRACT: Highly reflective crystals of the nucleotide base guanine are widely distributed in animal coloration and visual systems. Organisms precisely control the morphology and organization of the crystals to optimize different optical effects, but little is known about how this is achieved. Here we examine a fundamental question that has remained unanswered after over 100 years of research on guanine: *what are the crystals made of*? Using solution-state and solid-state chemical techniques coupled with structural analysis by powder XRD and solid-state NMR, we compare the purine compositions and the structures of seven biogenic guanine crystals with different crystal morphologies, testing the hypothesis that intracrystalline dopants influence the crystal shape. We find that biogenic "guanine" crystals are not pure crystals but *molecular alloys* (aka solid solutions and mixed crystals) of guanine, hypoxanthine, and sometimes xanthine. Guanine host crystals occlude homogeneous mixtures of other purines, sometimes in remarkably large amounts (up to 20% of hypoxanthine), without significantly altering the crystal structure of the guanine host. We find no correlation between the biogenic crystal morphology and dopant content and conclude that dopants do not dictate the crystal morphology of the guanine host. The ability of guanine crystals to host other molecules enables animals to build physiologically "cheaper" crystals from mixtures of metabolically available purines, without impeding optical functionality. The exceptional levels of doping in biogenic guanine offer inspiration for the design of mixed molecular crystals that incorporate multiple functionalities in a single material.
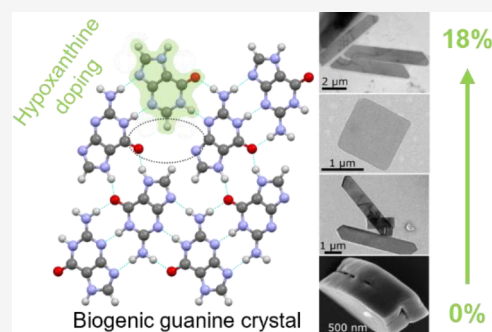
INTRODUCTION

Highly reflective guanine crystals are responsible for a diverse array of optical phenomena in animal coloration[1,2] and vision.[3−7] Biogenic guanine crystals are found in the β-polymorph,[8] which comprises π-stacked, planar arrays of H-bonded molecules[8] (Figure 1). Their optical utility derives from the extreme in-plane refractive index (n = 1.83).[9,10] The thermodynamically favored α-polymorph differs only in the direction of the stacking offset.[11] Organisms produce a striking array of different guanine crystal morphologies to optimize specific optical effects[12] (Figure 2). For example, narrow[13−15] and broad-band[16−18] reflectivity is produced by constructive interference from multilayers of plate crystals, in which the highly reflective but thermodynamically disfavored (100) face (parallel to the H-bonded plane) is preferentially expressed.[19] White colors in spiders result from diffuse scattering from randomly arranged micrometer-sized guanine prisms.[20−22] 3D-photonic crystals constructed from blocky guanine crystals produce light-induced color changes in chameleons.[23] Non-iridescent blue colors in certain lizards arise from scattering from disorganized arrays of premature, nanosized guanine crystals.[24]

Almost nothing is known about how the morphology of guanine crystals is precisely controlled. Tackling this question is important to our understanding of "organic biomineralization" and has the potential to yield new, bioinspired approaches for controlling the crystallization of synthetic materials. One hypothesis is that organisms utilize other purine molecules as intracrystalline growth additives to affect the morphology.[1,25] It was suggested that hypoxanthine (Figure 1b) and xanthine may inhibit growth along the π-stacking direction, promoting the formation of platelike crystals.[1,26−28] Several studies reported the presence of hypoxanthine in guanine-containing tissues in fish,[25,29−31] frogs,[32,33] and nudibranchs.[34] Adenine was also reported in frog integument.[33] In most cases it could not be ascertained whether the molecules were present in the solid state or as solutes in the
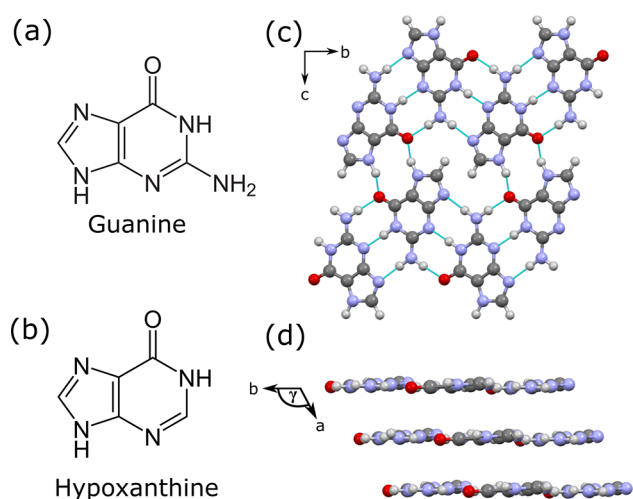
Figure 1. Molecular structures of (a) guanine and (b) hypoxanthine. The crystal structure of β-guanine viewed (c) perpendicular to the H-bonding layer and (d) along the *c* axis, showing the stacking of the planar H-bonded guanine layers.

crystal-forming cells. The relationship between crystal composition and morphology remained ambiguous.

Here, we evaluate the purine compositions and structural properties of biogenic guanine crystals with different crystal morphologies. We show that biogenic "guanine" crystals are in fact solid solutions of guanine and hypoxanthine and sometimes xanthine. In some cases, remarkably large amounts (ca. 20 mol %) of hypoxanthine are accommodated within the β-guanine host crystals without altering the crystal structure.

We find no correlation between the crystal morphology and hypoxanthine content and conclude that dopants do not dictate the biogenic guanine morphology. Instead, we hypothesize that the ability of guanine crystals to occlude other purine molecules enables organisms to build physiologically "cheaper" crystals without impeding their optical functionality. Guanine host crystals offer inspiration for the design of mixed crystals in which the crystal properties (i.e., optical) could be tuned by manipulating dopant composition.

■ RESULTS

We first collected (see Materials and Methods in the Supporting Information) guanine crystals from model species, and their morphologies were characterized by scanning electron microscopy (SEM) and transmission electron microscopy (TEM) (Figure 2 and Figures S1−S3). The crystals were face-indexed using electron diffraction. Species were chosen to enable a large variety of crystal morphologies across a range of animal phyla to be studied. Synthetic β-guanine[35] and synthetic β-guanine−hypoxanthine mixed crystals were also investigated as controls.

Guanine crystals from white spiders *Latrodectus pallidus* (*pallidus*) and *Argiope lobata* (*lobata*) (Figure 2a,b) are prismatic. The crystals are usually observed as "doublets" in which two crystals are adjoined by their (100) faces. Each prism is typically 200−500 nm thick and ca. 1 μm wide.

Crystals from silver *C. deserticola* (*deserticola*) spiders (Figure 2c) are thin ca. 20 nm[20] polygonal plates. They are assembled into doublets (70 nm thick in total) attached to each other by a noncrystalline material.[20] Some elongated hexagonal crystals were also found in this sample (Figure S1). Crystals from
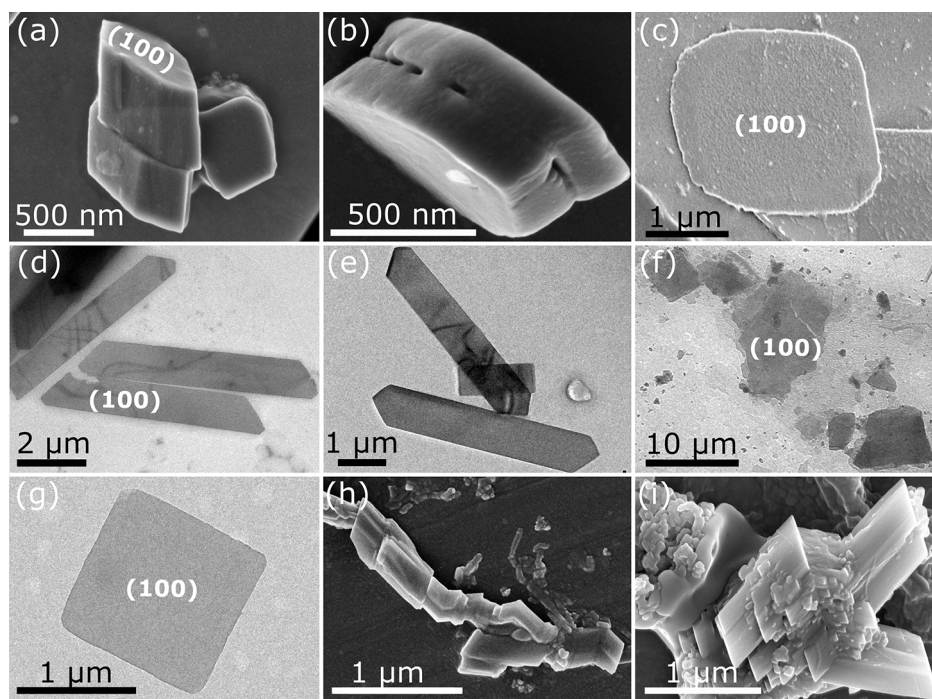

Figure 2. Morphologies of biogenic guanine crystals by SEM and TEM. (a, b) Prismatic guanine crystals from the white spiders *L. pallidus* (a) and *A. lobata* (b). The prisms are arranged into doublets attached by the (100) face. (c) An irregular polygonal plate from the integument of the silver *C. deserticola* spider. Elongated hexagonal crystal plates from the skin of fish *S. salar* (d) and *D. labrax* (e). (f) Large irregular polygonal plates from the wall of the swim bladder of the fish *S. pilchardus*. (g) Square plates from the eye of the scallop *P. maximus*. (h) Synthetic β-guanine crystals, twinned along the (100) face. (i) β-Guanine−hypoxanthine mixed crystals, displaying a prismatic morphology elongated along the *a* axis, and occasionally twinned along the (100) face. The (100) face is denoted for each unique biogenic guanine morphology.
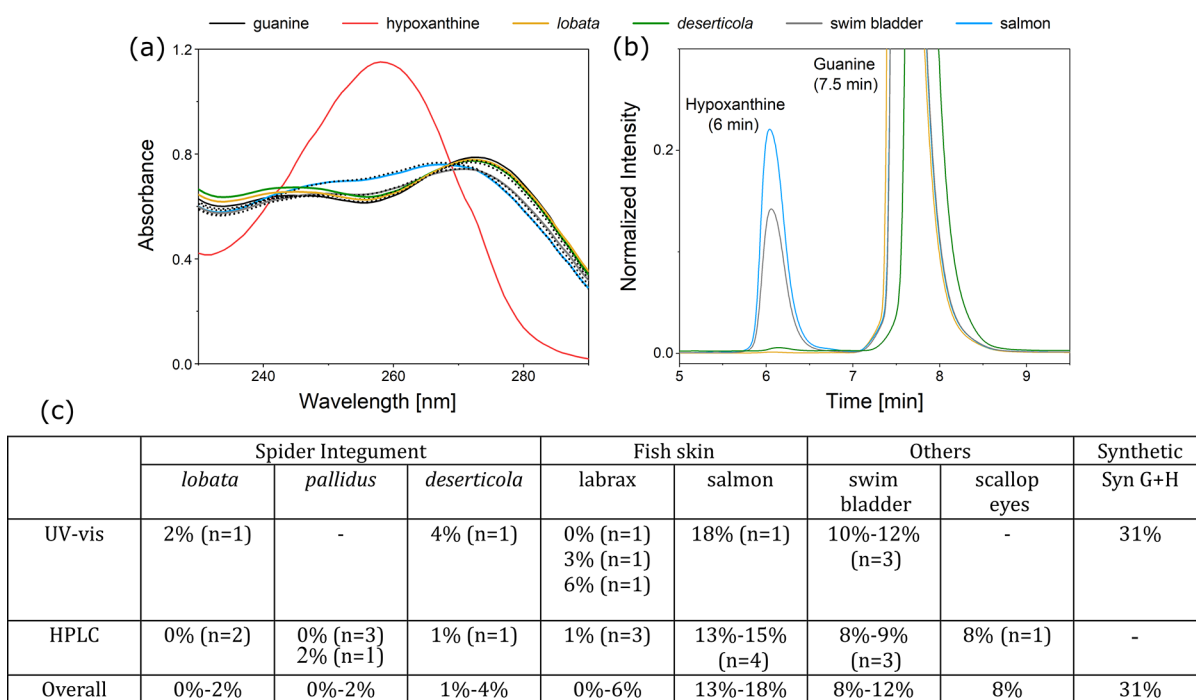
Figure 3. Chemical composition of biogenic guanine crystals. (a) UV−vis spectra of purified biogenic guanine crystals and standards of guanine and hypoxanthine $(10^{-4}$ M). Fits of these spectra were used to derive the guanine:hypoxanthine ratio of the biogenic crystals. Experimental spectra are shown by solid-colored traces. Simulated spectra are denoted by black dotted traces. (b) HPLC of purified biogenic guanine crystals. The guanine and hypoxanthine retention times were 6 and 7.5 min, respectively. The area under the peaks was integrated, and the guanine:hypoxanthine ratio was determined by comparison with calibration measurements. (c) Summary of the hypoxanthine content of the biogenic crystals (mol %) determined from both UV−vis and HPLC. n denotes the number of different samples measured. β-Guanine−hypoxanthine mixed crystals are denoted as "Syn G+H".

Salmo salar (salmon) and *Dicentrarchus labrax* (labrax) skin are thin (ca. 25 nm[20]) hexagonal plates elongated along the *b* axis (Figure 2d,e). A mixture of irregular polygonal plates and elongated hexagons (like those from fish skin) were extracted from the swim bladder of the sardine, *Sardina pilchardus* (swim bladder) (Figure 2f and Figure S2). The swim bladder is an internal organ in fish that controls buoyancy.[36] It is covered by a silvery layer of guanine crystals that serves as a diffusion barrier to gases.[37,38] The (100) plate face of the polygons varies between 2 and 50 μm in width. In TEM, the crystals, found in stacks, are more transparent in comparison to plates from fish skin, indicating they are thinner (<20 nm) (Figure S3f). Crystals from the eyes of scallops (*Pecten maximus*) are 75 nm thick, 1.2 μm wide squares, twinned twice about the ⟨021⟩ axis[39] (Figure 2g). The synthetic β-guanine crystals are prisms elongated along the *a* axis and are arranged into stacks of crystals twinned about the (100) face (Figure 2h). The synthetic β-guanine−hypoxanthine mixed crystals (Figure 2i) exhibit a variety of crystal morphologies but are usually prisms elongated along the *a* axis (resembling pure synthetic β-guanine) and occasionally twinned along the (100) faces.

Raman spectra (Figure S4) obtained from single crystals or powders of the biogenic crystals confirms that all biogenic crystals are of the β-guanine polymorph. In addition to the characteristic β-guanine modes,[40] peaks at 1321 and 1399 cm^{-1} are also present in crystals from salmon and the swim bladder. Moreover, a relatively intense (in comparison to the β-guanine standard) band at 725 cm^{-1} is also present in these crystals. This peak coincides with the intense pyrimidine ring-breathing mode of hypoxanthine.[41] All of these additional

Raman peaks are also found in the β-guanine−hypoxanthine mixed crystals.

To determine the purine composition of the biogenic crystals, crystals were first rigorously purified (Supporting Information). The purified crystals were dissolved in buffer (NH$_4$OH/NH$_4$Cl, pH 10.4), and their UV−vis spectra were measured (Figure 3a and Figures S5 and S6). Under the same conditions, the UV−vis spectra of guanine and hypoxanthine standards $(10^{-4}$ M) were recorded. The guanine:hypoxanthine ratio of the biogenic crystals was then determined by fitting the spectra to the absorbance of the two standards at their λ_{max} values ($\lambda_{guanine}$ = 273 nm, $\lambda_{hypoxanthine}$ = 258 nm). According to the calculated guanine:hypoxanthine ratio a simulated spectrum was generated for each biogenic sample. The close agreement between the experimental UV−vis spectra and the two-component guanine:hypoxanthine fits suggests that the biogenic crystals are primarily binary mixtures of guanine and hypoxanthine. For a more definitive determination of the crystal composition, high-pressure liquid chromatography (HPLC) (Figure 3b and Figures S7−S9 and Tables S1 and S2) was performed. The hypoxanthine percentage of the biogenic crystals was determined by comparing the hypoxanthine:guanine peak area ratios with respect to a calibration curve (Figure S8). The compositions of the biogenic crystals are shown in Figure 3c. Hypoxanthine was detected in small amounts (<2%) in prismatic crystals from the two white spiders (*pallidus* and *lobata*). At these low percentages, the UV−vis absorption curve is similar to the guanine standard and thus accurately quantifying the hypoxanthine amount is difficult. In crystals from silver spiders (*deserticola*), <1% of hypoxanthine was detected by HPLC, whereas 4% was
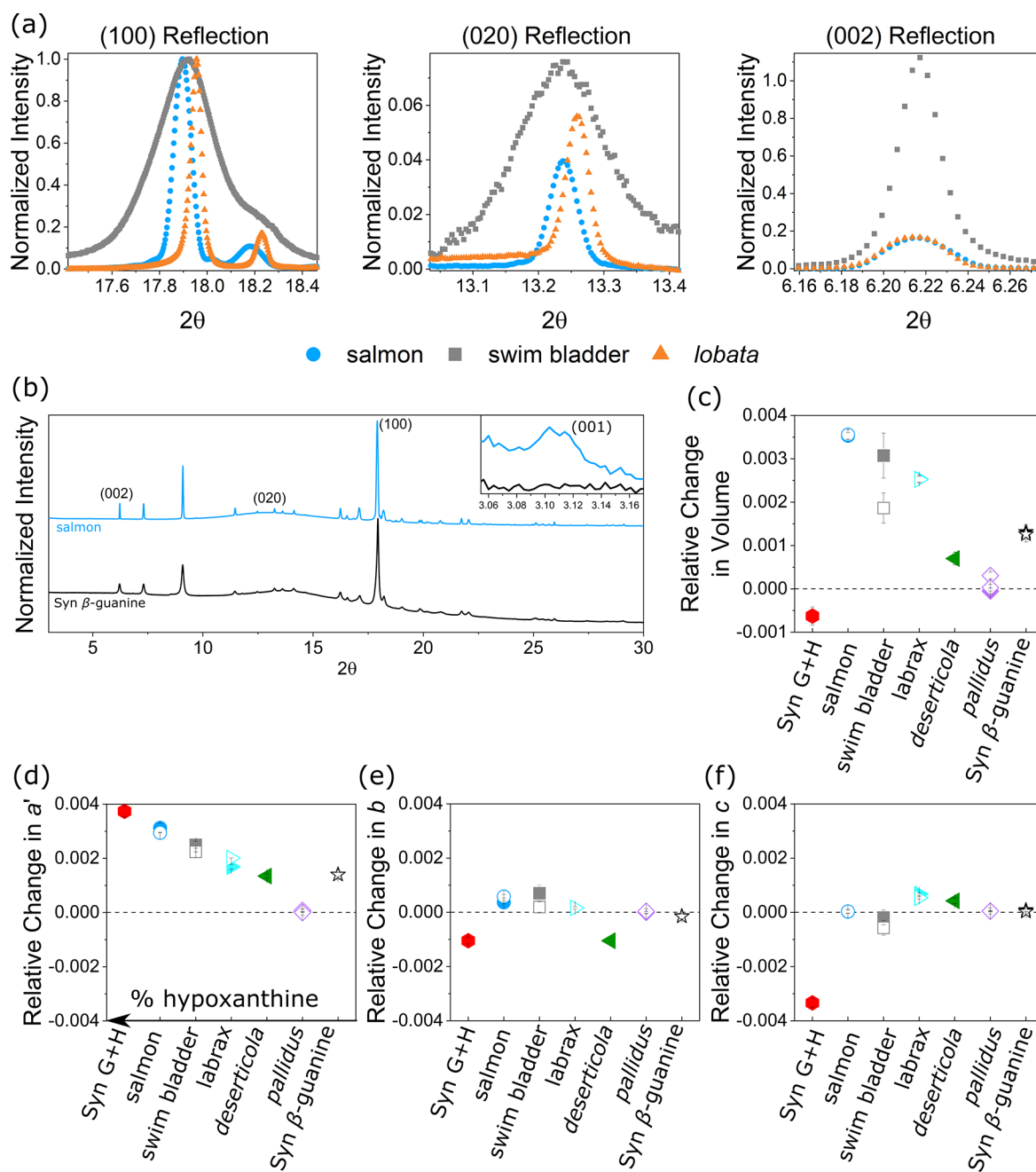
Figure 4. High-resolution synchrotron powder XRD data and analysis. (a) The (100), (020), and (002) reflections of the β-guanine structure observed in crystals from salmon, swim bladder and the *lobata* spider. The (100) and (020) peaks in crystals from salmon and swim bladder are shifted toward lower angles. (b) Examples of powder XRD patterns of salmon guanine and synthetic β-guanine. Inset: the symmetry-forbidden (001) peak present in the salmon pattern. (c–f) Plots of the relative change in unit cell parameters of biogenic and synthetic guanine crystals with respect to those of the white spider *lobata* obtained by Rietvled refinement (Table S3): (c) volume, (d) the distance, *a′*, between H-bonding sheets and (e) the *b*-axis and (f) *c*-axis. Synthetic β-guanine is denoted "Syn β-guanine", and β-guanine−hypoxanthine mixed crystals is denoted "Syn G +H". Filled and hollow data points of the same color and shape represent data points from different samples of the same species.

observed by UV−vis. The fitting obtained for this particular UV−vis spectrum was relatively poor, indicating the presence of other molecules affecting the absorbance. Thus, the actual hypoxanthine quantity may be lower than that measured. Crystals from labrax skin have 0−6% hypoxanthine by UV−vis and 1% by HPLC. Guanine from the swim bladder and salmon skin have the highest hypoxanthine content, with 8−12% and 13−18% of hypoxanthine, respectively. In one out of four samples of crystals from salmon skin, ca. 3% of xanthine was detected by HPLC. Hypoxanthine (8%) was also detected in

scallop eyes. The β-guanine−hypoxanthine mixed crystals contain 31% of hypoxanthine by UV−vis.

To rationalize how hypoxanthine is accommodated within the guanine crystals, a detailed structural analysis was performed on the basis of synchrotron powder XRD[42] data (Figure 4 and Figures S10−S12 and Tables S3−S7). Powder XRD patterns show that all biogenic samples are β-guanine (Figure 4b). No peaks corresponding to either the monoclinic[43] or triclinic[44] phases of pure hypoxanthine were observed in any of the PXRD patterns (Figure S11). In

addition to the normal β-guanine diffraction pattern, crystals from salmon, swim bladder, and β-guanine−hypoxanthine mixed crystals exhibit a weak peak at $2\theta = 3.1°$, corresponding to the (001) reflection (Figure 4b, inset). In the $P2_1/b$ space group, this reflection is symmetry forbidden due to the 2_1 screw axis. High amounts of hypoxanthine doping are the likely cause of this symmetry breaking. Powder XRD of crystals from the two white spiders and labrax contain up to 14% of α-guanine, and the silver spider *deserticola* has 39% of α-guanine. The α-guanine is probably produced by a solid-state transformation of the β-polymorph to the thermodynamically stable[8] α-polymorph during crystal purification. Since guanine is insoluble in water, we rule out the possibility that the β-polymorph dissolves and recrystallizes to the α-polymorph during cleaning. This is evidenced by the fact that the cleaned crystals retain the original crystal morphology and exhibit smooth (i.e., non-etched) surfaces when they are observed by SEM. We observe significant shifts in the peak positions between the different biogenic crystals (Figure 4a), with the positions of the (100) and (020) reflections being shifted to higher d spacing in samples containing hypoxanthine, whereas the position of the (002) reflection remains constant.

To quantify these variations in lattice parameters and to ascertain whether lattice distortions are correlated with hypoxanthine content, we performed a Rietveld refinement of the powder XRD data using the crystal structure of β-guanine as the structural model (Figure S10). Two-phase refinements were performed for samples containing both the β-phase and the α-phase. The refined unit cell parameters are shown in Table S3. To elucidate the effect of hypoxanthine inclusion in the guanine crystal structure, the relative difference between the lattice parameters of the biogenic crystals and those of *lobata* (where hypoxanthine is absent or present only in trace amounts) are shown in Figure 4c−f. Perhaps surprisingly, crystals containing more hypoxanthine have higher unit cell volumes, even though hypoxanthine has a lower molecular volume compared to guanine. This may be due to the presence of structural water in hypoxanthine-doped biogenic guanine crystals (see ss-NMR results and the Discussion). To rationalize these lattice distortions, we note that the perpendicular distance between the H-bonded layers, (denoted as a' and defined as $a' = a \cos(\gamma - 90°)$) is affected by hypoxanthine inclusion. Specifically, a' increases with increasing hypoxanthine content, meaning that hypoxanthine inclusion is associated with an expansion of the unit cell along the [100] stacking direction. Along the unique c axis, the lattice distortions are very small. The unit cell volume of pure synthetic β-guanine is higher than that of crystals from white and silver spiders, which contain little to no hypoxanthine. Synthetic β-guanine−hypoxanthine mixed crystals have the highest value of a' out of all samples. However, they have significantly lower values of b, c, and unit cell volume in comparison to biogenic crystals containing hypoxanthine.

To determine whether the inclusion of hypoxanthine is associated with an increase in crystal microstrain, line-shape analysis of the powder-XRD data was performed (Figure S12 and Tables S4−S7). Pseudo-Voigt fitting was used to decouple Gaussian and Lorentzian components of the peak profile, which provide information on average crystallite size and microstrain, respectively.[45] No correlation was found between strain and hypoxanthine content. However, the microstrain along the [100] direction is inversely correlated with the thickness of the crystals; thin crystals from the swim bladder

have the highest microstrain, and thick prismatic crystals from white spider *lobata* have the lowest microstrain. In comparison to the other biogenic crystals, the reflections from the swim bladder are significantly broader, except for the (00l) reflections, which have very sharp Lorentzian line shapes. Line broadening of the (100) peak in the swim bladder is consistent with these crystals being extremely thin plates.

To further explore evidence for the incorporation of purines within biogenic guanine crystals, solid-state nuclear magnetic resonance (ss-NMR) experiments were performed. High-resolution ^{13}C NMR spectra of biogenic guanine from the swim bladder are compared with spectra of polycrystalline synthetic β-guanine and hypoxanthine standards (Figure 5). Figure 5a also shows $^1H \rightarrow ^{13}C$ cross-polarization spectra (recorded with magic-angle spinning and high-power ^1H decoupling) for the swim bladder and the synthetic β-guanine and hypoxanthine standards. All lines in the spectra of the β-guanine and hypoxanthine standards are assigned, with chemical shifts being comparable to previously reported
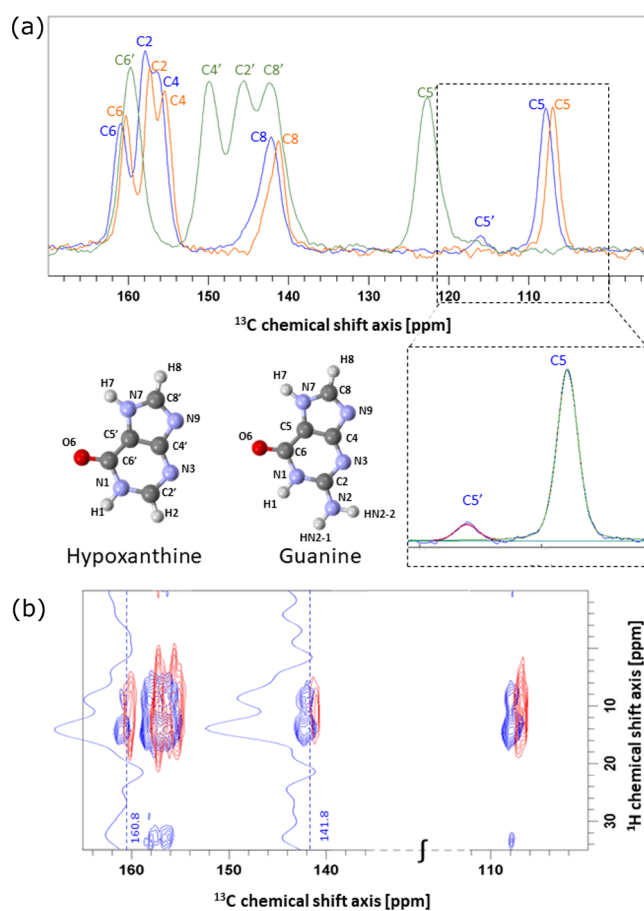

Figure 5. (a) ^{13}C CPMAS (cross-polarization magic angle spinning) spectra of the swim bladder (blue), synthetic β-guanine (orange) and hypoxanthine (green). Assigned carbons are color-coded on the basis of the color of the spectrum. Hypoxanthine lines are additionally marked with a prime (Cn', n = 2, 4, 5, 6, 8). Inset: enlargement of a deconvolution of the C5/C5$'$ region of the swim bladder ^{13}C spectrum. The annotated guanine and hypoxanthine structures correspond to the spectral labeling. (b) 2D ^1H−^{13}C heteronuclear correlation spectra of the swim bladder (blue) and synthetic β-guanine (red). 1D projections at 141.8 ppm and at 160.8 ppm (marked with vertical dashed lines) along the carbon chemical shift axis are overlaid on the 2D spectra (Figure S14).

values.[46,47] The ^{13}C spectrum of the swim bladder crystals exhibits resonances attributable to the β-guanine component of the sample. An additional peak at 116 ppm is attributed to the C5′ carbon of hypoxanthine. This peak has a unique resonance frequency distinct from any peaks characteristic of guanine. Using a standard line fitting of the C5′/C5 peaks of hypoxanthine and guanine, we calculate an intensity ratio of 8:92 for C5′:C5. This indicates that ca. 8% of the intensity in the ^{13}C NMR spectrum of the swim bladder crystals originates from hypoxanthine (Figure 5a, inset), in agreement with results from solution-state UV–vis and HPLC (Figure 3). Furthermore, the ^{13}C resonances for the guanine component of the swim bladder crystals are shifted downfield with respect to the ^{13}C resonances in pure synthetic β-guanine, indicating that they are affected by the presence of the hypoxanthine molecules inside the crystal.

^{1}H NMR spectra for the three samples (Table 1 and Figure S13) show overlapped bands representing the −NH and −CH

Table 1. Solid-State NMR Peak Assignments of the ^{1}H and [13]C Lines

atom	swim bladder (ppm)	β-guanine (ppm)	Δ β-guanine (ppm)	hypoxanthine (ppm)
C2	157.9	157.4	0.5	145.8
C4	156.4	155.5	0.9	149.9
C5 (C5′)	107 (116)	107.1	−0.1	122.8
C6	161	160.4	0.6	159.6
C8	142.2	141.4	0.8	142.4
H1, H9, HN	14.9	14.2	0.7	14.0, 16.7
H2, H8	8.7	7.8	0.9	8.15

protons in guanine and hypoxanthine and a water line at ca. 5.0 ppm. A line at 0.75 ppm is also observed in the swim bladder crystals, which is attributed to phospholipid protons originating from the crystal forming cells. Deconvolution of the swim bladder ^{1}H NMR spectrum into individual computed ^{1}H resonances (Figure S14) indicates that 19% of the protons are from water molecules. 2D [1]H−[13]C CP-based heteronuclear correlation spectra for swim bladder and β-guanine (Figure 5b) indicate that the ^{13}C resonances due to guanine in the swim bladder are shifted slightly downfield. They also indicate a slightly better resolution of the −NH protons from the −CH protons. Projections taken along the ^{1}H axis at the C2 (160.8 ppm) and C8 (141.8 ppm) chemical shifts (Figure 5b, dashed lines) are overlaid on the 2D spectra (Figure 5b, blue). They indicate that water protons are involved in polarizing the guanine carbons in the swim bladder crystals, confirming the presence of water molecules occluded within the crystals. Deconvolution of these 1D slices into individual lines (Figure S14) shows the fraction of water protons out of the total polarizing proton intensity is ca. 7.4%. This demonstrates that a significant amount of structural water resides within the hypoxanthine-doped swim bladder crystals. Analogous HET-COR spectra of the synthetic β-guanine and hypoxanthine standards show no evidence of intracrystalline water.

■ DISCUSSION

Guanine crystals have been found in a huge variety of optical systems in animals[1] as well as in some nonoptical "devices" (e.g., the swim bladder[38]). They have also been found widely in many unicellular eukaryotes, where they mainly function as high-turnover nitrogen reservoirs.[40,48,49]

Little is known about how the substituent guanine crystals in these systems are formed. Even the most fundamental question, "what are guanine crystals made of?", has remained ambiguous. It was shown previously that hypoxanthine and sometimes adenine are present in guanine-forming tissues. Due to the absence of solid-state methodologies or adequate crystal purification, these studies could not decipher whether the "additives" are present as solutes or as intracrystalline dopants.

Our results show that biogenic guanine crystals are not pure molecular crystals but are actually solid solutions composed of homogeneous mixtures of guanine, hypoxanthine and sometimes xanthine. While solid solutions in synthetic molecular crystals[50−54] and inorganic biominerals[55−57] have been widely studied, this phenomenon has not been found before in biogenic molecular crystals. Further work is required to determine whether this observation is a widespread phenomenon in other biogenic organic crystals such as isoxanthopterin[58,59] and 7,8-dihydroxanthopterin.[60]

The hypoxanthine content of the biological guanine crystals varies significantly from none (or trace quantities) in crystals from *lobata* and *pallidus* to ca. 12 and ca. 18% in swim bladder and salmon crystals, respectively. In the last two cases, it is remarkable that such high amounts of hypoxanthine are accommodated within the guanine crystals without significantly altering the crystal structure. In salmon crystals, on average, almost every unit cell contains one molecule of hypoxanthine. Such doping levels are rarely observed in synthetic molecular mixed crystals in which the two pure crystalline phases are not isostructural[61−63] (Figure 6). We observe that, when large amounts of hypoxanthine are included within the guanine crystal, symmetry breaking occurs and the symmetry-forbidden (001) peak is present in the powder XRD data. The relatively low intensity of this reflection suggests random, nonselective occlusion of hypoxanthine molecules within the β-guanine crystal structure.

Powder XRD analysis shows that, for both biogenic and synthetic mixed crystals, the inclusion of hypoxanthine is correlated with an increase in the *d* spacing between H-bonded guanine layers. The out-of-plane[64] NH2 group in the optimized geometry of the guanine molecule becomes planar when it is inside the crystal due to its participation in H-bonding. In the β-guanine crystal structure, each molecule is bound to four neighboring guanine molecules by eight hydrogen bonds. Thus, the loss of two out of eight H-bonds (Figure 6a,b) upon the inclusion of every hypoxanthine molecule may be responsible for the loss in planarity of the guanine layers (Figure 6c,e). A second explanation is the preference of hypoxanthine to adopt a slightly corrugated H-bond arrangement (Figure 6d), as observed in the pure monoclinic phase of hypoxanthine (Figure 6d,f).[43]

Additionally, the crystallization of synthetic β-guanine−hypoxanthine mixed crystals in the β-guanine phase (Figure S10h) agrees with a recent finding that guanine preferentially crystallizes as the β-polymorph[65] when it forms solid solutions with hypoxanthine and xanthine. This suggests that purine additives may stabilize the metastable β-polymorph. A similar effect was recently observed when the metastable benzamide form III was stabilized upon forming solid solutions with the nonisostructural additive nicotinamide.[63] Since the replacement of guanine by hypoxanthine involves replacement of an −NH2 group by H on the N2 of guanine (Figure 6b), we expect that hypoxanthine inclusion should result in lattice contraction within the *bc* plane and a decrease in the unit cell
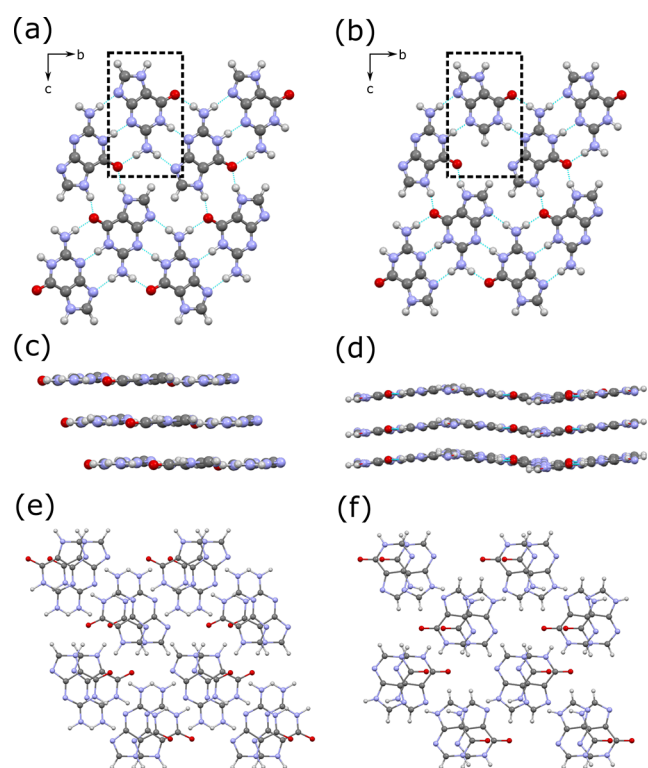
Figure 6. Structural comparison of the packing of pure β-guanine ($P2_1/b$, a = 3.63 Å, b = 9.81 Å, c = 18.43 Å, γ = 118.04°), hypoxanthine-doped β-guanine, and pure monoclinic hypoxanthine ($P2_1/c$, a = 3.67 Å, b = 17.91 Å, c = 9.01 Å, β = 107.47°). (a) H-bonding layer of pure β-guanine. The dashed box shows the NH_2 group participating in two (out of eight) H-bonds. (b) H-bonding layer of β-guanine with one guanine molecule substituted by a hypoxanthine molecule. The NH_2 group of the guanine is essentially replaced by a H atom and two H-bonds are lost. (c) Packing of the planar β-guanine H-bonding layers. (d) Packing of the nonplanar H-bonding layers of the monoclinic hypoxanthine crystal structure.[43] Crystal packing of β-guanine (e) and hypoxanthine (f) viewed perpendicular to the H-bonding layer.

volume. As predicted, the b and c axes and unit cell volume of synthetic β-guanine−hypoxanthine mixed crystals are lower than those of the synthetic β-guanine standard. Surprisingly, in biogenic crystals, hypoxanthine inclusion is instead associated with lattice expansion along the b axis and increased unit cell volume. We cannot fully rationalize this behavior, but our ss-NMR analysis suggests that, in the presence of hypoxanthine, water is included in the crystal structure. This structural water may compensate for the missing H-bonds, giving rise to unit cell expansion. Another possibility is the presence of nonpurine additives in the crystal.

Interestingly, line-shape analysis of the (100) peak (corresponding to π−π stacking) shows a correlation between the thickness of the crystals and the microstrain along the [100] direction. The extremely thin swim bladder crystals have the highest microstrain, followed by crystals from salmon (ca. 25 nm thick) and the silver spider (ca. 20−30 nm thick). Thick prismatic crystals from the white spider *lobata* exhibit the lowest microstain. Previous work shows that growth rates of crystals are impeded along directions of high microstrain,[66] suggesting that the thickness of guanine crystals studied in this work may be related to strain.

No correlation was found between biogenic crystal morphology (in particular, thickness), and hypoxanthine content. The observation of similar amounts of hypoxanthine in thick (>200 nm) crystals from *lobata* and *pallidus* and thin (ca. 20 nm) crystals from *deserticola* contradicts the hypothesis that hypoxanthine inhibits growth along the stacking direction. The large variation in hypoxanthine content within the thin crystals also shows that intracrystalline dopants do not directly, or proportionally, dictate morphology. For example, salmon and labrax contain similar (ca. 25 nm thick) elongated hexagonal plates but very different hypoxanthine contents (13−18% and 0−6%, respectively). Moreover, the extremely thin crystals from the swim bladder contain less hypoxanthine (8−12%) in comparison to the thicker salmon crystals. Interestingly, the amount of hypoxanthine detected in crystals is often found to vary across a certain range between measurements. For example, in labrax, the hypoxanthine content varies between 0 and 6%, indicating that the crystal composition is not "genetically fixed" and there may be variation within individuals of the same species or even temporal variation in one individual. Our results do not preclude the possibility that nonoccluded purine additives influence the crystal morphology. However, it seems likely that organisms control crystal morphology by other, as yet unknown, strategies that are independent of purine chemistry.

This raises the question; what function, if any, does intracrystalline hypoxanthine have in biogenic guanine materials? We hypothesize that the ability of guanine crystals to accommodate high quantities of "foreign" purine molecules enables organisms to build physiologically "cheaper" crystals, without impeding optical functionality. Guanine and hypoxanthine are products of related nucleotide degradation pathways. In fish, they are both directly degraded to xanthine[67,68] before being catabolized to other nitrogenous waste products, which could explain the presence of xanthine in some salmon crystals. Conversely, in spiders, guanine is the end product of the nucleotide degradation pathway[68−70] and is excreted as waste or deposited in the guanophores.[68] It has been suggested that hypoxanthine production has been lost or impeded in spiders through evolution[70]—consistent with the finding that hypoxanthine is a minor component of spider guanine crystals. Thus, it seems that organisms "make use of what they have", building their crystals from mixtures of structurally similar purines available from nitrogen metabolism. We suspect that the purine composition of "guanine" crystals *simply* reflects the natural metabolism of the organism. Previous studies showed that, by preferentially orienting the (100) face of guanine (parallel to the high refractive index, H-bonded plane) toward the incident light, the reflectivity is enhanced.[25,71] Since hypoxanthine can be incorporated without disturbing the crystal structure or morphology (and thus the resulting optimized optical properties), organisms can "freely" vary crystal composition according to their metabolic profile. The refractive index of crystals is governed by the polarizability of the substituent molecules.[10] Since hypoxanthine and guanine have very similar polarizabilities,[64] hypoxanthine doping is unlikely to substantially change the refractive index or degrade the optical functionality of the crystals.

■ CONCLUSIONS

Since its discovery in silvery fish scales over 130 years ago,[72] most studies have treated biogenic guanine as a pure crystalline

phase. Our results show that "guanine" crystals are complex materials, which exist as solid solutions of guanine and other purines. We conclude that intracrystalline dopants do not dictate the morphology of biogenic guanine crystals but that organisms use other "strategies" to control crystallization. The remarkable flexibility of guanine crystals to *host* purine molecules enables animals to efficiently build crystals from structurally similar purines available in the crystal-forming cells. The exceptional levels of doping in biogenic guanine offer inspiration for engineering mixed molecular crystals that incorporate multiple functionalities in a single material.

ASSOCIATED CONTENT

Supporting Information

The Supporting Information is available free of charge at https://pubs.acs.org/doi/10.1021/jacs.2c00724.

> Materials and experimental details, SEM, TEM diffraction patterns, Raman spectroscopy, UV−vis spectroscopy, HPLC chromatograms and data, powder XRD analysis, and ss-NMR spectra (PDF)

AUTHOR INFORMATION

Corresponding Author

Benjamin A. Palmer − *Department of Chemistry, Ben-Gurion University of the Negev, Be'er Sheba 8410501, Israel;* orcid.org/0000-0002-9684-9724; Email: bpalmer@bgu.ac.il

Authors

Noam Pinsk − *Department of Chemistry, Ben-Gurion University of the Negev, Be'er Sheba 8410501, Israel*

Avital Wagner − *Department of Chemistry, Ben-Gurion University of the Negev, Be'er Sheba 8410501, Israel*

Lilian Cohen − *Department of Chemistry, Bar-Ilan University, 5290002 Ramat Gan, Israel*

Christopher J. H. Smalley − *School of Chemistry, Cardiff University, Cardiff CF10 3AT Wales, United Kingdom;* orcid.org/0000-0003-2088-6921

Colan E. Hughes − *School of Chemistry, Cardiff University, Cardiff CF10 3AT Wales, United Kingdom*

Gan Zhang − *Department of Chemistry, Ben-Gurion University of the Negev, Be'er Sheba 8410501, Israel;* orcid.org/0000-0002-3651-3196

Mariela J. Pavan − *Ilse Katz Institute for Nanoscale Science & Technology, Ben-Gurion University of the Negev, Be'er Sheba 8410501, Israel*

Nicola Casati − *Paul Scherrer Institute, 5232 Villigen PSI, Switzerland;* orcid.org/0000-0002-4206-9239

Anne Jantschke − *Institute of Geosciences, Johannes-Gutenberg-Universität, 55128 Mainz, Germany*

Gil Goobes − *Department of Chemistry, Bar-Ilan University, 5290002 Ramat Gan, Israel*

Kenneth D. M. Harris − *School of Chemistry, Cardiff University, Cardiff CF10 3AT Wales, United Kingdom;* orcid.org/0000-0001-7855-8598

Complete contact information is available at:
https://pubs.acs.org/10.1021/jacs.2c00724

Notes

The authors declare no competing financial interest.

REFERENCES

(1) Gur, D.; Palmer, B. A.; Weiner, S.; Addadi, L. Light Manipulation by Guanine Crystals in Organisms: Biogenic Scatterers, Mirrors, Multilayer Reflectors and Photonic Crystals. *Adv. Funct. Mater.* **2017**, *27*, 1603514.

(2) Land, M. F. The Physics and Biology of Animal Reflectors. *Prog. Biophys.* **1972**, *24*, 75−106.

(3) Palmer, B. A.; Gur, D.; Weiner, S.; Addadi, L.; Oron, D. The Organic Crystalline Materials of Vision: Structure−Function Considerations from the Nanometer to the Millimeter Scale. *Adv. Mater.* **2018**, *30*, 1800006.

(4) Palmer, B. A.; Taylor, G. J.; Brumfeld, V.; Gur, D.; Shemesh, M.; Elad, N.; Osherov, A.; Oron, D.; Weiner, S.; Addadi, L. The Image-Forming Mirror in the Eye of the Scallop. *Science.* **2017**, *358*, 1172−1175.

(5) Mueller, K. P.; Labhart, T. Polarizing Optics in a Spider Eye. *J. Comp. Physiol.* **2010**, *196* (5), 335−348.

(6) Gur, D.; Nicolas, J. D.; Brumfeld, V.; Bar-Elli, O.; Oron, D.; Levkowitz, G. The Dual Functional Reflecting Iris of the Zebrafish. *Adv. Sci.* **2018**, *5* (8), 1800338.

(7) Wagner, H. J.; Douglas, R. H.; Frank, T. M.; Roberts, N. W.; Partridge, J. C. A Novel Vertebrate Eye Using Both Refractive and Reflective Optics. *Curr. Biol.* **2009**, *19* (2), 108−114.

(8) Hirsch, A.; Gur, D.; Polishchuk, I.; Levy, D.; Pokroy, B.; Cruz-Cabeza, A. J.; Addadi, L.; Kronik, L.; Leiserowitz, L. Guanigma": The Revised Structure of Biogenic Anhydrous Guanine. *Chem. Mater.* **2015**, *27* (24), 8289−8297.

(9) Huxley, A. F. A High-Power Interference Microscope. *J. Physiol.* **1954**, *125*, 11−3P.

(10) Wagner, A.; Wen, Q.; Pinsk, N.; Palmer, B. A. Functional Molecular Crystals in Biology. *Isr. J. Chem.* **2021**, *61* (9), 668−678.

(11) Guille, K.; Clegg, W. Anhydrous Guanine: A Synchrotron Study. *Acta Crystallogr. C* **2006**, *62* (8), o515−o517.

(12) Kinoshita, S.; Yoshioka, S.; Miyazaki, J. Physics of Structural Colors. *Rep. Prog. Phys.* **2008**, *71* (7), 076401.

(13) Lythgoe, J. N.; Shand, J. Changes in Spectral Reflexions from the Iridophores of the Neon Tetra. *J. Physiol.* **1982**, *325* (1), 23−34.

(14) Gur, D.; Leshem, B.; Pierantoni, M.; Farstey, V.; Oron, D.; Weiner, S.; Addadi, L. Structural Basis for the Brilliant Colors of the Sapphirinid Copepods. *J. Am. Chem. Soc.* **2015**, *137* (26), 8408−8411.

(15) Gur, D.; Palmer, B. A.; Leshem, B.; Oron, D.; Fratzl, P.; Weiner, S.; Addadi, L. The Mechanism of Color Change in the Neon Tetra Fish: A Light-Induced Tunable Photonic Crystal Array. *Angew. Chem., Int. Ed.* **2015**, *127* (42), 12603−12607.

(16) Jordan, T. M.; Partridge, J. C.; Roberts, N. W. Non-Polarizing Broadband Multilayer Reflectors in Fish. *Nat. Photonics* **2012**, *6* (11), 759−763.

(17) Denton, E. J.; Land, M. F. Mechanism of Reflexion in Silvery Layers of Fish and Cephalopods. *Proc. Royal Soc. B* **1971**, *178* (50), 43−61.

(18) Denton, E. J.; Nicol, F. R. S.; Nicol, J. A. C. Studies on Reflexion of Light from Silvery Surfaces of Fishes, with Special Reference to the Bleak, Alburnus Alburnus. *J. Mar. Biol.* **1965**, *45*, 683−703.

(19) Levy-Lior, A.; Pokroy, B.; Levavi-Sivan, B.; Leiserowitz, L.; Werner, S.; Addadi, L. Biogenic Guanine Crystals from the Skin of Fish May Be Designed to Enhance Light Reflectance. *Cryst. Growth Des.* **2008**, *8* (2), 507−511.

(20) Levy-Lior, A.; Shimoni, E.; Schwartz, O.; Gavish-Regev, E.; Oron, D.; Oxford, G.; Weiner, S.; Addadi, L. Guanine-Based Biogenic Photonic-Crystal Arrays in Fish and Spiders. *Adv. Funct. Mater.* **2010**, *20* (2), 320−329.

(21) Oxford, G. S. Guanine as a Colorant in Spiders: Development, Genetics, Phylogenetics and Ecology. *Proceedings of the 17th European Colloquium of Arachnology, Edinburgh*, 1997.

(22) Insausti, T. C.; Casas, J. The Functional Morphology of Color Changing in a Spider: Development of Ommochrome Pigment Granules. *J. Exp. Biol.* **2008**, *211* (5), 780−789.

(23) Teyssier, J.; Saenko, S. v.; van der Marel, D.; Milinkovitch, M. C. Photonic Crystals Cause Active Colour Change in Chameleons. *Nat. Commun.* **2015**, *6* (1), 1−7.

(24) Zhang, G.; Yallapragada, V. J.; Shemesh, M.; Wagner, A.; Upcher, A.; Pinkas, I.; McClelland, H. L. O.; Hawlena, D.; Palmer, B. A. Ontogenetic Color Switching in Lizards as a By-Product of Guanine Cell Development. *bioRxiv.* **2022**, 2022.01.12.475993.

(25) Greenstein, L. M. Nacreous Pigments and Their Properties. *Toilet Goods Association* **1966**, *46*, 20−26.

(26) Ma, Y.; Chen, F.; Hu, Y.; Liu, Y.; Qi, L. Controlled Crystallization of Twinned Crystalline Guanine Microplatelets. *CrystEngComm* **2019**, *21* (42), 6346−6353.

(27) Gur, D.; Addadi, L.; Weiner, S. Synthetic Co-Crystals of Anhydrous Guanine and Process for Preparing the Same, WO2017/221245 A1, 2016.

(28) Wu, B.; Liu, Y.; Chen, F.; Li, J.; Yu, Y.; Zhou, Y.; Li, L.; Xiao, J.; Ma, Y. Investigation on the Formation Mechanism of Twinned Crystals of Hypoxanthine-Doped Beta-Phase Anhydrous Guanine Microplatelets. *CrystEngComm* **2021**, *23* (19), 3444−3452.

(29) Johnston, C. E.; Eales, J. G. Purines in the Integument of the Atlantic Salmon (Salmo Salar) During Parr-Smolt Transformation. *J. Fish. Res.* **1967**, *24* (5), 955−964.

(30) Mcfall-Ngai, M. J. Adaptations for Reflection of Bioluminescent Light in the Gas Bladder of Leiognathus Equulus (Perciformes: Leiognathidae). *J. Exp. Zool.* **1983**, *227* (1), 23−33.

(31) Aihara, M.; Kasukawa, H.; Fujii, R.; Oshima, N. Chemical Characterization of Reflecting Platelets in Motile Iridophores of Blue Damselfish. *Comp. Biochem. Physiol. B, Biochem. Mol. Biol.* **1989**, *92* (3), 533−536.

(32) Ide, H.; Hama, T. Guanine Formation in Isolated Iridophores from Bullfrog Tadpoles. *Biochim. Biophys. Acta* **1972**, *286* (2), 269−271.

(33) Taylor, J. D. The Effects of Intermedin on the Ultrastructure of Amphibian Iridophores. *Gen. Comp. Endrocrinol.* **1969**, *12* (3), 405−416.

(34) Dearden, S. J.; Ghoshal, A.; Demartini, D. G.; Morse, D. E. Sparkling Reflective Stacks of Purine Crystals in the Nudibranch Flabellina Iodinea. *Biol. Bull.* **2018**, *234* (2), 116−129.

(35) Gur, D.; Pierantoni, M.; Elool Dov, N.; Hirsh, A.; Feldman, Y.; Weiner, S.; Addadi, L. Guanine Crystallization in Aqueous Solutions Enables Control over Crystal Size and Polymorphism. *Cryst. Growth Des.* **2016**, *16* (9), 4975−4980.

(36) Kutchai, H.; Steen, J. B. The Permeability of the Swimbladder. *Comp. Biochem. Physiol.* **1971**, *39* (1), 119−123.

(37) Ross, L. G. The Permeability to Oxygen of the Swimbladder of the Mesopelagic Fish Ceratoscopelus Maderensis. *Mar. Biol.* **1976**, *37* (1), 83−87.

(38) Denton, E. J.; Liddicoat, J. D.; Taylor, D. W. The Permeability to Gases of the Swimbladder of the Conger Eel (Conger Conger). *J. Mar. Biolog. Assoc. U.K.* **1972**, *52* (3), 727−746.

(39) Hirsch, A.; Palmer, B. A.; Elad, N.; Gur, D.; Weiner, S.; Addadi, L.; Kronik, L.; Leiserowitz, L. Biologically Controlled Morphology and Twinning in Guanine Crystals. *Angew. Chem., Int. Ed.* **2017**, *129* (32), 9548−9552.

(40) Jantschke, A.; Pinkas, I.; Hirsch, A.; Elad, N.; Schertel, A.; Addadi, L.; Weiner, S. Anhydrous *β*-Guanine Crystals in a Marine Dinoflagellate: Structure and Suggested Function. *J. Struct. Biol.* **2019**, *207* (1), 12−20.

(41) Huang, W.; Jiang, J. Z.; Chen, L.; Zhang, B. Q.; Deng, S. F.; Sun, J. J.; Chen, W. K. Density Functional Theory and Surface Enhanced Raman Spectroscopy Studies of Tautomeric Hypoxanthine and Its Adsorption Behaviors in Electrochemical Processes. *Electrochim. Acta* **2015**, *164*, 132−138.

(42) Willmott, P. R.; Meister, D.; Leake, S. J.; Lange, M.; Bergamaschi, A.; Böge, M.; Calvi, M.; Cancellieri, C.; Casati, N.; Cervellino, A.; Chen, Q.; David, C.; Flechsig, U.; Gozzo, F.; Henrich, B.; Jäggi-Spielmann, S.; Jakob, B.; Kalichava, I.; Karvinen, P.; Krempasky, J.; Lüdeke, A.; Lüscher, R.; Maag, S.; Quitmann, C.; Reinle-Schmitt, M. L.; Schmidt, T.; Schmitt, B.; Streun, A.; Vartiainen, I.; Vitins, M.; Wang, X.; Wullschleger, R. The Materials Science Beamline Upgrade at the Swiss Light Source. *J. Synchrotron Radiat.* **2013**, *20* (5), 667−682.

(43) Yang, R. Q.; Xie, Y. R. A Monoclinic Polymorph of Hypoxanthine. *Acta Crystallogr. E* **2007**, *63* (7), o3309−o3309.

(44) Schmalle, H. W.; Hänggi, G.; Dubler, E. Structure of Hypoxanthine. *Acta Crystallogr. C* **1988**, *44* (4), 732−736.

(45) Zolotoyabko, E.; Quintana, J. P. Non-Destructive Microstructural Analysis with Depth Resolution: Application to Seashells. *J. Appl. Crystallogr.* **2002**, *35* (5), 594−599.

(46) Maliňáková, K.; Novosadová, L.; Lahtinen, M.; Kolehmainen, E.; Brus, J.; Marek, R. 13C Chemical Shift Tensors in Hypoxanthine and 6-Mercaptopurine: Effects of Substitution, Tautomerism, and Intermolecular Interactions. *J. Phys. Chem. A* **2010**, *114* (4), 1985−1995.

(47) Reid, J.; Bond, T.; Wang, S.; Zhou, J.; Hu, A. Synchrotron Powder Diffraction, X-Ray Absorption and 1H Nuclear Magnetic Resonance Data for Hypoxanthine, $C_5H_4N_4O$. *Powder Diffr.* **2015**, *30* (3), 278−285.

(48) Mojzeš, P.; Gao, L.; Ismagulova, T.; Pilátová, J.; Moudříková, Š.; Gorelova, O.; Solovchenko, A.; Nedbal, L.; Salih, A. Guanine, a High-Capacity and Rapid-Turnover Nitrogen Reserve in Microalgal Cells. *Proc. Natl. Acad. Sci. U.S.A.* **2020**, *117* (51), 32722−32730.

(49) Pilátová, J.; Pánek, T.; Oborník, M.; Čepička, I.; Mojzeš, P. Paradigm Shift in Eukaryotic Biocrystallization. *bioRxiv* **2022**, 2022.01.11.475817.

(50) Lusi, M. Engineering Crystal Properties through Solid Solutions. *Cryst. Growth Des.* **2018**, *18* (6), 3704−3712.

(51) Cruz-Cabeza, A. J.; Lestari, M.; Lusi, M. Cocrystals Help Break the "Rules" of Isostructurality: Solid Solutions and Polymorphism in the Malic/Tartaric Acid System. *Cryst. Growth Des.* **2018**, *18* (2), 855−863.

(52) Nauha, E.; Naumov, P.; Lusi, M. Fine-Tuning of a Thermosalient Phase Transition by Solid Solutions. *CrystEngComm* **2016**, *18* (25), 4699−4703.

(53) Saha, S.; Mishra, M. K.; Reddy, C. M.; Desiraju, G. R. From Molecules to Interactions to Crystal Engineering: Mechanical Properties of Organic Solids. *Acc. Chem. Res.* **2018**, *51* (11), 2957−2967.

(54) Liu, F.; Hooks, D. E.; Li, N.; Rubinson, J. F.; Wacker, J. N.; Swift, J. A. Molecular Crystal Mechanical Properties Altered via Dopant Inclusion. *Chem. Mater.* **2020**, *32* (9), 3952−3959.

(55) Davis, K. J.; Dove, P. M.; de Yoreo, J. J. The Role of Mg^{2+} as an Impurity in Calcite Growth. *Science* **2000**, *290* (5494), 1134−1137.

(56) Seknazi, E.; Pokroy, B. Residual Strain and Stress in Biocrystals. *Adv. Mater.* **2018**, *30* (41), 1707263.

(57) Ma, Y.; Aichmayer, B.; Paris, O.; Fratzl, P.; Meibom, A.; Metzler, R. A.; Politi, Y.; Addadi, L.; Gilbert, P. U. P. A.; Weiner, S. The Grinding Tip of the Sea Urchin Tooth Exhibits Exquisite Control over Calcite Crystal Orientation and Mg Distribution. *Proc. Natl. Acad. Sci. U.S.A.* **2009**, *106* (15), 6048−6053.

(58) Palmer, B. A.; Hirsch, A.; Brumfeld, V.; Aflalo, E. D.; Pinkas, I.; Sagi, A.; Rosenne, S.; Oron, D.; Leiserowitz, L.; Kronik, L.; Weiner, S.; Addadi, L. Optically Functional Isoxanthopterin Crystals in the Mirrored Eyes of Decapod Crustaceans. *Proc. Natl. Acad. Sci. U.S.A.* **2018**, *115* (10), 2299−2304.

(59) Palmer, B. A.; Yallapragada, V. J.; Schiffmann, N.; Wormser, E. M.; Elad, N.; Aflalo, E. D.; Sagi, A.; Weiner, S.; Addadi, L.; Oron, D. A Highly Reflective Biogenic Photonic Material from Core−Shell Birefringent Nanoparticles. *Nat. Nanotechnol.* **2020**, *15* (2), 138−144.

(60) Zhang, G.; Hirsch, A.; Shmul, G.; Avram, L.; Elad, N.; Brumfeld, V.; Pinkas, I.; Feldman, Y.; Ben Asher, R.; Palmer, B. A.; Kronik, L.; Leiserowitz, L.; Weiner, S.; Addadi, L. Guanine and 7,8-Dihydroxanthopterin Reflecting Crystals in the Zander Fish Eye: Crystal Locations, Compositions, and Structures. *J. Am. Chem. Soc.* **2019**, *141* (50), 19736−19745.

(61) Kitaigorodsky, A. I.; *Mixed Crystals*; Springer-Verlag: 1984; Vol. 33.

(62) Kitaigorodskii, A. I. *Physical Chemistry*; Academic Press: 1973; Vol. 29 (Molecular Crystals and Molecules).

(63) Kras, W.; Carletta, A.; Montis, R.; Sullivan, R. A.; Cruz-Cabeza, A. J. Switching Polymorph Stabilities with Impurities Provides a Thermodynamic Route to Benzamide Form III. *Commun. Chem.* **2021**, *4* (1), 1−7.

(64) Johnson, R. C.; Power, T. D.; Holt, J. S.; Immaraporn, B.; Monat, J. E.; Sissoko, A. A.; Yanik, M. M.; Zagorodny, A. V.; Cybulski, S. M. Electron-Correlated Calculations of Electric Properties of Nucleic Acid Bases. *J. Phys. Chem.* **1996**, *100* (48), 18875−18881.

(65) Chen, F.; Guo, D.; Gao, J.; Ma, Y. Bioinspired Crystallization of Guanine. *J. Phys. Chem. Lett.* **2021**, *12* (48), 11695−11702.

(66) Brice, J. C. Some Thermodynamic Aspects of the Growth of Strained Crystals. *J. Cryst. Growth* **1975**, *28* (2), 249−253.

(67) Balinsky, J. B. Phylogenetic Aspects of Purine Metabolism. *S. Afr. Med. J.* **1972**, 993−997.

(68) Keilin, J. The Biological Significance of Uric Acid and Guanine Excretion. *Biol. Rev.* **1959**, *34* (3), 265−294.

(69) Haggag, G.; Fouad, Y. Nitrogenous Excretion in Arachnids. *Nature* **1965**, *207* (5000), 1003−1004.

(70) Anderson, J. F. The Excreta of Spiders. *Comparative Biochemistry and Physiology* **1966**, *17* (3), 973−982.

(71) Funt, N.; Palmer, B. A.; Weiner, S.; Addadi, L. Koi Fish-Scale Iridophore Cells Orient Guanine Crystals to Maximize Light Reflection. *ChemPlusChem.* **2017**, *82* (6), 914−923.

(72) Cunningham, J. T.; MacMunn, C. A. On the Coloration of the Skins of Fishes, Especially of Pleuronectidæ. *Philos. Trans. R. Soc. B* **1893**, *184*, 765−812.